On estimation of local mass burning rates for steady laminar boundary layer diffusion flames

Ajay V. Singh and Michael J. Gollner

University of Maryland College Park, College Park, Department of Fire Protection Engineering, 3106 J.M. Patterson Bldg., College Park, Maryland 20742, United States

Corresponding Author: Michael J. Gollner
Department of Fire Protection Engineering
University of Maryland, College Park
3106 J.M. Patterson Bldg.
College Park, MD 20742
U.S.A.
Email: mgollner@umd.edu
Phone: +1 (301) 405-6667
Fax: +1 (301) 405-9383

Preferred Colloquium: Fire Research

Paper Length: **5784 words** (16 available, *Method 1*)
Text = 3886 words
Equations = 183 words
Equation 1 = (2 lines + 2 blank) × 7.6 words/line × 1 = 30.4
Equation 2 = (2 lines + 2 blank) × 7.6 words/line × 1 = 30.4
Equation 3 = (2 lines + 2 blank) × 7.6 words/line × 1 = 30.4
Equation 4 = (2 lines + 2 blank) × 7.6 words/line × 1 = 30.4
Equation 5 = (2 lines + 2 blank) × 7.6 words/line × 1 = 30.4
Equation 6 = (2 lines + 2 blank) × 7.6 words/line × 1 = 30.4
References = 507 words
(27+2) × 2.3 × 7.6 = 560
Tables = 304 words
Table 1 = (8+2) × 7.6 × 2 = 152
Table 2 = (8+2) × 7.6 × 2 = 152
Figures & Captions = 904 words
Figure 1 – (55.626 +10) × 2.2 × 1 + 64 = 209
Figure 2 – (63.246 +10) × 2.2 × 2 + 22 = 345
Figure 3 – (64.262+10) × 2.2 × 2 + 23 = 350

Abstract Length: 209 words (91 available)

Color Reproduction: Not Required

Supplemental Material: Attached

Keywords: laminar burning, diffusion flame, vertical wall, flame spread

Abstract:

A thorough numerical and experimental investigation of laminar boundary-layer diffusion flames established over the surface of a condensed fuel is presented. By extension of the Reynold's Analogy, it is hypothesized that the non-dimensional temperature gradient at the surface of a condensed fuel is related to the local mass-burning rate through some constant of proportionality. First, this proportionality is tested by using a validated numerical model for a steady flame established over a condensed fuel surface, under free and forced convective conditions. Second, the relationship is tested by conducting experiments in a free-convective environment (vertical wall) using methanol and ethanol as liquid fuels and PMMA as a solid fuel, where a detailed temperature profile is mapped during steady burning using fine-wire thermocouples mounted to a precision two-axis traverse mechanism. The results from the present study suggests that there is indeed a unique correlation between the mass burning rates of liquid/solid fuels and the temperature gradients at the fuel surface. The correlating factor depends upon the Spalding mass transfer number and gas-phase thermo-physical properties and works in the prediction of both integrated as well as local variations of the mass burning rate as a function of non-dimensional temperature gradient. Additional results from precise measurements of the thermal field are also presented.

1. Introduction

In most problems related to fire safety, the mass-burning rate is a key parameter to evaluate the ability of a material to influence fire growth, since it plays a fundamental role in determining fire size and flame spread. Knowledge of local mass burning rates provides increased experimental information on the burning of condensed fuels, enabling more insight into the mechanisms which affect small scale burning. While measurements of the average burning rate of a condensed fuel are readily available, local burning rate measurements are difficult to determine, even in small-scale experiments [1-2]. The work presented here has utilized numerical and experimental data of steady laminar flames established over condensed fuel surfaces to first verify that a relationship exists between the non-dimensional temperature gradient at the fuel surface and the local mass-burning rate. This relationship is essentially a further extension of the Chilton-Colburn extension [3] to the Reynold's Analogy [4] to relate heat, momentum and mass transfer. For laminar buoyant and forced-convective configurations, numerical and experimental results show that the relationship remains valid for both solid and liquid fuels and should prove useful for the study of laminar burning fuels and future numerical validation, as the laminar wall fire is a canonical fire research problem.

2. Literature Review

The modern era of studies on boundary-layer diffusion flames with application to fire safety began with the mathematical modeling of a steady flame in a forced flow airstream carried out by Emmons [5]. A similarity solution of the classical reacting boundary layer problem under a zero-gravity environment was reported. Due to the simplicity of the closed-form equation, Emmon's classical solution has been used widely and provided a starting point for similar solutions of steady [6-8] and spreading [9] laminar flames. These studies all consider the steady small-scale burning of flat plates using the laminar boundary layer (LBL) approximation, which relies on a similarity hypothesis and the flame-sheet approximation. The results of these analyses supports experimental evidence that the local burning rate

per unit area decreases with distance from the leading edge and is controlled by the fuel mass-transfer number, B and the flow geometry [10, 11].

Several experimental studies have investigated steady, boundary-layer type diffusion flames. Hirano and co-authors [12, 13], injected gaseous fuels uniformly through a porous flat plate into a parallel air stream, mimicking Emmon's configuration. Subsequently Hirano and Kinoshita [14] measured gas velocities and temperature profiles across a methanol diffusion flame and later, Andreussi and Petarca [15] using ethyl alcohol as a fuel. While both studies provided increased insight on the laminar burning of fuel surfaces in a forced flow, only one configuration reported by Hirano [14] provides local temperatures of sufficient accuracy for the proposed approach, however, no attempt was made to measure the local fuel consumption rate. While there have been several relevant studies on the laminar burning of polymethyl methacrylate (PMMA) slabs [16-19], only Ananth et al. [1] and later Ndubizu et al. [2] report both average burning rates and temperature profiles for steady and unsteady PMMA burning in a laminar forced convective environment. All previous experimental studies reporting local temperatures, therefore, have focused exclusively on a forced flow configuration similar to Emmons [5]. Recently, Ali and co-workers [20] reported numerical results on estimation of laminar mass burning rate using temperature field in a free convective environment. However, no experiments were conducted to support the numerical results. The work presented here has utilized both numerical and experimental data of steady laminar flames established over condensed fuel surfaces to verify that a unique relationship exists between the non-dimensional temperature gradient at the fuel surface and the local mass-burning rate.

3. Theoretical Formulation

The method proposed here has its basis in the work of Chilton-Colburn [3] and Silver [4] whose extension to the Reynolds' analogy establishes a relationship between mass, momentum, and heat transfer in a boundary layer over a solid or liquid fuel surface and is given by

$$\frac{\tau_s}{u_\infty \nu^{2/3}} \equiv \frac{h}{c_p \alpha^{2/3}} \equiv \frac{\dot{m}''}{D^{2/3} \ln(1+B)}, \quad (1)$$

where ν is the kinematic viscosity or momentum diffusivity, α represents the thermal diffusivity, and D is the species diffusivity. Equation (1) implies that the shear stress at the surface τ_s is related to the heat transfer (h/c_p) and mass transfer from combustion, $\dot{m}''$. The terms u_∞, h, and c_p are the free-stream velocity, heat-transfer coefficient, and the specific heat of the gas, respectively. The term B that appears in Eq. (1) is a non-dimensional proportionality constant that relates the rate of mass transfer (e.g., vaporization, combustion) to the rate of heat transfer and shear stress, essentially the driving force for mass transfer, and was first referred to as the "transfer number" by Spalding [10].

The logarithmic function of B in Eq. (1) is due to the stagnant film hypothesis and more exact functions of B than $\ln(1+B)$ can be derived in particular cases by solving the typical differential equations and boundary conditions of mass transfer. For example, Emmons [5] used the relationship between the shear stress and mass-burning rate (the first and third term in Eq. (1)) to analyze the film combustion of a flat fuel surface in a forced convective flow field. Following Chilton-Colburn's relationship [3], Emmons [5] hypothesized that the shear stress at the surface of a combusting fuel must be proportional to the mass-burning rate. Emmons mathematically proved that if such proportionality exists, the constant of proportionality is the mass transfer or B-number. In other words,

$$\dot{m}_f'' = B \frac{\tau_s}{u_\infty}, \quad (2)$$

where, $\tau_s = \mu\left(\partial u/\partial y + \partial v/\partial x\right)_{y=0}$. If the value of B is known, Eq. (2) allows for the prediction of the mass burning rate when the gas-phase shear stress at the surface is known. This approach provides a conceptual convenience for modeling a phenomenon like fuel pyrolysis, since there is no need to explicitly account for the interaction between the gas and liquid phases. This relationship works for non-

deforming, non-charring fuels as well, as long as more complicated chemical-kinetic effects are neglected.

Based on Chilton-Colburn's equation, a relationship between mass and heat transfer also exists. This relationship originates from the fact that processes in which material is transferred by diffusion are closely related to heat transfer, since the latter can be considered merely as the diffusion of hot molecules into a region of cold ones and a corresponding diffusion of cold molecules in the reverse direction. Since the mechanism is so similar, it would be expected that a relationship could be obtained for diffusional processes entirely analogous to that for heat transfer. The heat transfer coefficient at the surface of a flat fuel can then be expressed as,

$$h = \frac{k}{L}\left(\frac{\partial T^*}{\partial y^*}\right)_{y^*=0}, \tag{3}$$

where $T^* = T - T_\infty / T_\infty$ represents the non-dimensional temperature, T_∞ represents the ambient temperature, L is a length scale representing the length of the region that is pyrolyzing or vaporizing and $y^* = y / L$ denotes the non-dimensional normal direction with reference to the surface that is issuing fuel vapor. This non-dimensional temperature gradient is therefore analogous to the Nusselt number. Using Eqs. (1)-(3), and the assumption of a constant Prandtl number near the fuel surface, one can obtain the following relationship between the mass-burning rate and the temperature gradient,

$$\dot{m}''_f = \frac{C}{L}\left(\frac{\partial T^*}{\partial y^*}\right)_{y^*=0}, \tag{4}$$

where the proportionality constant C appearing in Eq. (4) equals Bk / c_p, where k is the thermal conductivity and c_p is the specific heat, both measured in the gas phase close to the surface of the fuel. Conceptually, Eq. (4) states that the proportionality between the velocity gradient at the surface (momentum transfer) and the fuel vaporization rate in a chemically reacting boundary layer will extend to the temperature gradient as well. A similar analysis can be performed to demonstrate the

proportionality between the fuel species and mass transfer using the assumption of a constant Schmidt number. For fire science, the utility of Eq. (4) is evident as it allows estimation of the local mass-burning rate by measurement of the temperature profiles along the fuel surface.

4. Numerical Simulations

Two-dimensional transient numerical simulations of laminar diffusion flames established over a methanol and ethanol pool under both a forced convective and a vertically-oriented free-convective environment were carried out using commercial CFD software, Fluent 6.3. The salient features of the numerical model include temperature and concentration-dependent thermo-physical properties, multi-component species diffusion, multi-step chemical kinetic mechanisms and a detailed Discrete Ordinates radiation model. Full multi-component diffusion along with a diffusion energy source is used to model the species diffusion. Skeletal mechanisms for methanol-air [21] and ethanol-air [22] diffusion flames are used. Grid sizes were chosen after a careful grid independence study, where a grid of 650×450 cells in the *x*- and *y*-directions provides a good balance between solution accuracy and computational economy for an 8 cm long burning surface (L = 8 cm). The boundary condition at the methanol pool interface was specified as a liquid-gas interface with a no-slip boundary condition for tangential velocity (*x*-direction velocity) and no liquid-phase heating effects at the film/pool surface. A user-defined function was used to create a mass source that is based on an energy balance at the surface of the fuel film. The energy balance across the liquid-gas interface is modeled by assuming that heat conduction from the flame to the liquid fuel surface is equal to the energy needed to vaporize the fuel. Radiation from flame and energy loss into the liquid pool are assumed to be negligible. The user-defined function was defined as $(\dot{m}/V) = k(\partial T/\partial y)/L_{eff}\,\Delta y$, where k is the thermal conductivity in W/m-K, dT/dy is the temperature gradient in K/m, $\dot{m}/V$ is the burning rate per unit volume (computational cell volume) in kg/m^3-s, L_{eff} is the effective latent heat of vaporization of the liquid fuel in J/Kg and Δy is the height of the row of fluid cells in m. This allows for the liquid film to be maintained at the interface at all times.

The resulting temperature field was used to compare the local temperature gradient to the local mass-burning rate, shown in Fig. 1 for methanol under different forced and free-convective (vertical fuel) environments. It was observed from both numerical and experimental results (experimental results were obtained using the experimental apparatus described in section 5) that the temperature profiles follow an exponential profile very close to the condensed fuel surface and then increases linearly towards the flame temperature. The normal non-dimensional temperature gradients at the fuel surface, $(\partial T^* / \partial y^*)\big|_{y=0}$ were therefore calculated from the slope at $y = 0$ of an exponential fit to the temperature distribution near the fuel surface. When the local non-dimensional temperature gradient at the fuel surface was plotted against the corresponding local mass burning rate along the fuel surface, it results in a linear correlation irrespective of the flow conditions, similar to that proposed by Eq. (4). The slope of the linear curve was found to be equal to 0.653 g/m^{2}s which is nearly equal to $Bk/c_p L$ for methanol, 0.637 g/m^{2}s, using appropriate average values of B = 2.7 [23], k = 0.0263 W/mK [24], c_p = 1394.5 J/kgK [24] and L = 0.08 m. Here, k is the thermal conductivity of air evaluated at an ambient temperature of 300 K and c_p is the specific heat of the air evaluated at the adiabatic flame temperature of methanol $T_{ad} = 2150$ K, following the methodology by Kim, de Ris and Kroesser [7] where the mean specific heat was evaluated at the adiabatic flame temperature of the given fuel.

[FIGURE 1 ABOUT HERE]

Averaged results from the previously-described numerical simulations and from the experimental study of Hirano are shown in Table 1. The reasonably close agreement between the measured and predicted averaged mass-loss rates demonstrate that they can in theory be obtained from careful temperature measurements in the gas phase near the fuel surface.

[TABLE 1 ABOUT HERE]

5. Experimental facility and instrumentation

An experimental set-up was constructed that enabled simultaneous measurements of average mass-loss rates and local temperature profiles above a condensed fuel surface. A 30.5 × 61 cm aluminum plate with a 1.27 cm thick sheet of ceramic fiber insulation board was mounted vertically on top of a load cell with a section 12.7 cm from the base of the surface of the insulating sheet cut out for the fuel sample. The liquid fuel wick was an 8 × 8 × 1.27 cm thick sheet of porous noncombustible material (Alkaline earth silicate wool). The liquid wick was selected so that it would allow the fuel to freely diffuse while being able to withstand the high temperatures of an open flame without deformation. Before use, any residual binders in the material were desiccated through baking or flaming. Aluminum foil was sealed to all interfaces of the wick except the top face using sodium silicate, to eliminate leakage. By surrounding this wick with a smooth transition to ceramic fiber insulation board, width effects were reduced. During testing, the wick was soaked with liquid fuel up to its point of saturation so that it gave a stable flame for the longest duration possible (enough to take precise temperature measurements). In the case of solid fuel burning, an 8 × 8 × 1.27 cm thick sheet of cast PMMA was used instead of a liquid wick, which was ignited by a standard blowtorch passed over the entire fuel surface for exactly 1 minute, where uniform ignition was observed to occur.

The fuel average mass-loss rate was measured by a precision load cell with a resolution of ±0.1 g. Following ignition, the mass-loss rate (indicated by the slope of the mass loss curve) of liquid wicks remained constant for the majority of the test time, however as the wick dried up, the mass-loss rate decreased. Measurements were therefore made in the early stages of the burning process (< 460 s) when the average mass-loss rate was constant. Average mass burning rates presented for PMMA were an average mass-loss rate during the period thermocouples sampled near the surface, as the mass burning rates did not reach a steady state yet. All mass-burning rates presented are averages of six tests at a given condition. The repeatability of these measurements were within 2% of the mean.

Precise temperature measurements were carried out using R-type Pt/Pt-Rh 13% micro thermocouples mounted to a set of computer-controlled Velmex X-Y unislides that could be moved precisely up and down along the flame length or left and right across the flame thickness with a maximum spatial resolution of 1.5 μm. Voltage signals from the thermocouple were acquired, conditioned and digitized through a National Instruments® NI 9214, which is a 24-bit high density 16-channel thermocouple input module which can be used up to 0.02°C measurement sensitivity. LabVIEW software was used to synchronize motor control and temperature data acquisition. Because the temperature gradient is very steep within the boundary layer and the flame standoff distance is small in laminar flames (~0.1 cm at the base to ~1.0 cm at the top), very fine movements were necessary. Through numerical testing, it was determined at least 22-36 measurements at 0.5 mm intervals should be made across the flame, to resolve accurate temperature profiles near the fuel surface. Measurements were taken at 0.25 mm spacings near the condensed fuel surface and then subsequently incrementing the spatial distance to 0.5 mm. Both 50 μm and 75 μm diameter thermocouples wires were used over the same sample in order to ensure accurate radiation corrections by reading the difference between these two at the same location and applying the correlation of Collis and Williams [25-2625]. For the 50 μm diameter thermocouple a typical radiation correction at 1700 K was found to be approximately +83 K. Since the thermocouples cross regions of high temperature gradients, the measurements are expected to include conduction errors, however they are expected to be small here (<1%) since the heat-transfer area (the cross section of the thermocouple) is very small, therefore no corrections were made in the data for conduction errors.

Unlike liquid wicks, as the PMMA sample burns its surface regresses with time, therefore it was necessary to complete the temperature mapping while the surface remained relatively flat, within approximately 150 s following uniform ignition. 5-point temperature measurements from the molten layer into the gas-phase at 0.25 mm intervals were recorded at 12 *x*-locations within 150 s of ignition.

PMMA samples were also burned for different time intervals to assess errors from surface regression and to calculate the local mass-burning rates for comparison [Section 2, sup. mat.].

During the experimental tests, the data acquisition system acquired temperatures at 100 samples per second, providing 100 samples to average per spatial point. Temperature measurements were taken at 360 distinct points over liquid samples and at 60 over solid samples. Reported temperatures are averages of at least three tests for methanol and ethanol and at least five tests for PMMA in a given condition and the maximum standard deviation is < 3% of the mean. The uncertainty in temperatures measured by the thermocouple (T_{tc}) are taken to be 0.25% of the measured value based on manufacturer's specifications. The accuracy of the Nusselt number correlation used to calculate the radiation loss from the thermocouple bead was reported to be within 5% [26] and the uncertainty in k due to different species is assumed to be 3%. The error in the thermocouple emissivity used (ε_{tc}) is also small, $<\pm 3\%$, except that ε_{tc} is linear with T_{tc} so any error in T_{tc} increases the uncertainty in ε_{tc}. The Platinum emissivity was calculated using Jakob's theoretical correlation, confirmed by experimental data [27-28] which reported the Pt emissivity uncertainty $<\pm 3\%$ when using the calculation. The uncertainty in gas temperature is then calculated from a quadratic sum of the uncertainties:

$$dT_g = \left[\left(\frac{\partial T_g}{\partial T_b} dT_b \right)^2 + \left(\frac{\partial T_g}{\partial \varepsilon} d\varepsilon \right)^2 + \left(\frac{\partial T_g}{\partial k} dk \right)^2 + \left(\frac{\partial T_g}{\partial Nu} Nu \right)^2 \right]^{1/2} \quad (5)$$

The maximum uncertainty in gas temperatures encountered in the flame zone is then found to be within ± 10 K.

6. Experimental Results

Using the experimental apparatus described in Section 5, measurements were taken for average mass-burning rates and local temperature profiles along condensed fuel surfaces. Observation of the temperature gradients normal to the fuel surface suggest that they are highest near the leading edge and

decrease further downstream. The peak temperatures at the flame front show a similar trend, reaching a maximum of 1915 K and 1888 K for the methanol and ethanol flames, respectively, ~10 mm downstream of the leading edge. The temperature of the condensed fuel surface also decreased with *x*, however this change was very slight. The average temperature at the wall was 335 K for methanol and 345 K for ethanol, both lower than the boiling points by about 2 K for methanol and 6 K for ethanol. In the current tests, the convective heat flux has been estimated to be several times higher at the leading edge than in the trailing section, ~25.3 kW/m^2 at $x = 10$ mm and ~12.1 kW/m^2 at $x = 80$ mm for a methanol flame and ~32.5 kW/m^2 at $x = 10$ mm and ~13.9 kW/m^2 at $x = 80$ mm for a PMMA flame. The expression for evaluating convective heat flux was approximated as, $h\Delta T \approx (k\Delta T/\delta) \approx k(T_f - T_w)/\delta$, where δ is the flame stand-off distance, T_f and T_w are the temperatures of the flame and wall at a given *x* location respectively and k is the thermal conductivity of the gas phase evaluated at a mean temperature. Thus, the local mass-loss rate from the fuel, driven by convective heat flux to the surface in these small, laminar flames, should similarly decrease with x.

Figure 2 shows the variation of normal non-dimensional temperature gradient along the fuel surface extracted from the experimental data of methanol, ethanol and PMMA. The temperature gradient normal to the fuel surface was found to be highest at the leading edge and lowest at the trailing edge (*x* = 80 mm). The local mass-burning rate should follow a similar trend, as is revealed by the calculated rates in Fig. (3). Averaging the non-dimensional temperature gradient for the entire fuel surface from data in Fig. (2), the average mass-burning rate is estimated to be 15.60 g/m^{2}s, 17.82 g/m^{2}s and 9.72 g/m^{2}s for methanol, ethanol and PMMA respectively, using Eq. (4). Appropriate average values of transport properties were used to calculate the constant *C* in Eq. (4) and are given in Table 2. It is to be noted that while Kim et. al. evaluated the value of *k* at the wall, for PMMA *k* at the wall would drastically change the results (T_{wall} for PMMA is approximately twice that of liquid fuels). This could be rectified if a time-dependent average B-number is chosen as opposed to adiabatic B-number for PMMA

following Rangwala et. al., [29] whose decreased B would compensate for the increased *k*. However we chose the most uniform methodology for liquid and solid fuels in this work. The mass-burning rate evaluated though the load cell data was found to be 16.67 g/m^{2}s, 17.58 g/m^{2}s and 8.90 g/m^{2}s for methanol, ethanol and PMMA respectively. The error in the estimation of the average mass-burning rate was therefore found to be -7.05%, +1.36% and +9.21 % for methanol, ethanol and PMMA respectively. Recall that the temperature measurements for liquid fuels were taken in a steady burning regime, determined by global mass-loss data, however for PMMA the measurements were carried out within the first 150 s (after the surface is uniformly ignited, while the surface was still relatively flat), therefore the mass-loss rate reported is an average for this 150 s region. In the PMMA case, even though solid fuel burning does not yet reach a steady state, the gas-phase reaches a steady state soon after uniform ignition. At the leading edge of the solid, where heat feedback is high, a local gas-phase steady state is achieved soon after ignition, before a significant valley is formed. In that period, approximately all the heat feedback is used to gasify the solid. Later, a valley is formed and the surface regression rate decreases with time (outlined in Section 2, sup. mat.). This suggests the heat reaching the surface is no longer steady at times later than those covered in this work. In-depth solid conduction and heating is a slower process as opposed to gas-phase heating which is fast and rapid. The same observations were made by Ndubizu et. al. [2] when they burnt PMMA slabs in forced convective environments. The reasonably close agreement between the measured and predicted values demonstrates that the mass-burning rate can be reasonably obtained from high spatially-resolved temperature measurements in the gas phase near the fuel surface.

[FIGURE 2 ABOUT HERE]

[TABLE 2 ABOUT HERE]

Figure 3 shows the variation of the local mass-burning rate for vertically-oriented methanol and ethanol flames. The theoretical correlation from Eq. (4) and the non-dimensional temperature gradients at the

condensed fuel surface were used to evaluate the local mass-burning rate at different locations along the fuel surface. Due to the availability of fresh oxidizer, higher convective heat feedback, higher temperature gradients and lower standoff distances near the leading edge, the local burning rate is highest here and subsequently decreases as we move downstream towards the trailing edge. The burning rate decreases, due to the lack of fresh oxidizer, lower convective heat feedback, lower temperature gradients and higher flame standoff distances at these locations. Also, the local mass-burning rate in both the methanol and ethanol cases is almost proportional to $x^{-1/4}$, confirming the power-law relationship for laminar natural convective burning on a vertical surface [6, 7]. The local mass-burning rate evaluated by using Eq. (4) was also compared against the theoretical mass-burning rate given by Kim, de Ris and Kroesser [7]. For laminar natural convection burning the average mass-burning rate was found to be [7],

$$\dot{m}'' = 3\left[\frac{\rho_w^2 \mu_w^2 L_v g \cos\phi}{4\overline{C}_p T_\infty x}\right]^{1/4} [-f(0)] \qquad (6)$$

where ρ_w represents the density of the gas phase at the wall, μ_w dynamic viscosity at the wall, L_v the effective heat of vaporization, g acceleration due to gravity, ϕ the angle from vertical, $\overline{C}_p$ the mean specific heat for free convection, T_∞ the ambient temperature and x the coordinate parallel to the fuel surface, where the transport properties are evaluated at the surface temperature, T_w. $-f(0)$ was numerically calculated for various liquid fuels elsewhere [7]. The close agreement in estimating the local mass burning-rates through the theoretical model and the correlation in Eq. (4) suggest that the proposed theoretical correlation works well in the prediction of both integrated as well as local variation of mass burning rate for laminar flames established over a condensed fuel surface. Factors causing the theoretical relationships from Kim et al. to overestimate the local mass burning rate might include assumptions of unity Lewis and Prandtl numbers, a lack of radiation effects and uncertainties associated

with the calculation of transport properties. The same factors were found to be responsible for under and over estimating the mass burning rates by using the theoretical correlation in Eq. (4).

[FIGURE 3 ABOUT HERE]

Unlike liquid fuels, for PMMA the local mass-burning rate can be approximated *a posteriori* by measuring the local surface regression over fixed intervals of time [30, Section 2, sup. mat.]. Using a PMMA density of 1190 kg/m^3 and measuring regression from samples burned for fixed 50 s time intervals after ignition the local mass-burning rate over time can be assessed. A smaller time step would be desirable, however errors in measuring regression profiles become too apparent when the time step is less than 50 s. The regression data between burnout times of 100 and 150 s were used to evaluate the local mass-burning rate in Fig. (3) for PMMA. Both the regression-measured and Eq. (4) calculated mass-burning rates follow a power law decay in x with exponent -0.35 and -0.37, respectively. The same power law relationship for local mass-burning rates was observed by Pizzo et. al. [30] for vertical PMMA slabs of length 2.5 to 20 cm. The departure from the $x^{-0.25}$ dependence predicted by the LBL theory could be due to a combination of the following reasons (1) the upstream influence on the flame by the stabilization zone since the flame is not long enough (compared to standoff distance) to escape such effects, (2) finite-rate chemical kinetics, (3) the variations of flame and surface temperatures with x preclude the self-similar solution of boundary layer, and (4) radiative feedback to the solid does not follow the boundary layer scaling rule. Jiang et. al. [31] also observed that downstream flame in case of PMMA, deviated from the self-similar boundary layer scaling relation. Jiang and co-authors [31] observed that much of the flow of oxygen into the flame zone came from the upstream instead of the side, as implied by the classical boundary-layer theory. They observed that the variation in flame standoff distance and the fuel vapor blowing rate with x does not follow the $x^{-0.25}$ dependence, as implied by the self-similar solution of the boundary layer. The close agreement, however, in estimating the local mass-burning rates by both the regression data and temperature gradients with Eq. (4) suggest

that the proposed theoretical correlation works well for non-charring solid fuels as the experimental mass burning rate was not used in any way to obtain the theoretical mass-burning rate

7. Conclusion

The results from the present study show that there is a unique correlation between the local mass-burning rate and the local temperature gradient at a condensed fuel surface. The correlating factor depends upon the Spalding transfer number and gas-phase thermo-physical properties and works in the prediction of both integrated as well as local variations of mass burning rate. Numerical and experimental results closely support the given theoretical correlation. The theoretical correlation is in excellent agreement with methanol, ethanol and PMMA burning data and works well in predicting both the average and local mass burning rates. The theoretical correlation agrees with methanol, ethanol and PMMA burning data to within 10% accuracy. The local mass burning rates and temperature gradients collected in this paper can also be useful in extracting the local convective heat fluxes and to extract more detailed information on the thermal characteristics of laminar boundary-layer diffusion flames.

References

[1] R. Ananth, C.C. Ndubizu, P.A. Tatem, *Combust. Flame* 135 (2003) 35-55.

[2] C.C. Ndubizu, R. Ananth, P.A. Tatem, *Combust. Flame* 141 (2005) 131-148.

[3] T.H. Chilton, E.I. Colburn, *Indust. Eng. Chem.* 26 (1934) 1183-1187.

[4] R.S. Silver, *Nature* 165 (1950) 725-726.

[5] H.W. Emmons, *Z. Angew. Math. Mech.* 36 (1956) 60-71.

[6] F.J. Kosdon, F.A. Williams, C. Buman, *Proc. Comb. Inst.* 12 (1969) 252-264.

[7] J.S. Kim, J. de Ris, F.W. Kroesser *Proc. Comb. Inst.* 13 (1971) 949-960.

[8] P.J. Pagni, T.M. Shih, *Proc. Comb. Inst.* 16 (1977) 1329-1343.

[9] K. Annamalai, M. Sibulkin, *Comb. Sci. Tech.* 19 (1979) 167-183.

[10] D.B. Spalding, Fuel, 29 (1950) 2-7.

[11] D.B. Spalding, *Some Fundamentals of Combustion*, Butterworths, London (1955)

[12] T. Hirano, K. Iwai, Y. Kanno, Astronautica Acta. 17 (1972) 811-818.

[13] T. Hirano, Y. Kanno, *Proc. Comb. Inst.* 14 (1973) 391-398.

[14] T. Hirano, M. Kinoshita, *Proc. Comb. Inst.* 15 (1975) 379–387.

[15] P. Andreussi and L. Petarca, *Proc. Comb. Inst.* 18 (1981) 1861-1869.

[16] L. Krishnamurthy, F.A. Williams, *Proc. Comb. Inst.* 14 (1973) 1151-1164.

[17] J.N. de Ris, *Proc. Comb. Inst.* 12 (1969) 241-252.

[18] L. Zhou, A.C. Fernandez-Pello, *Combust. Flame* 92 (1993) 45-59.

[19] L. Zhou, A.C. Fernandez-Pello, *Proc. Comb. Inst.* 24 (1992) 1721-1728.

[20] S.M. Ali, V. Raghavan, and A.S. Rangwala, *Proceedings of 21st National & 10th ISHMT-ASME Heat and Mass Transfer Conference* (2011) Dec 27-30

[21] J.Y. Chen, *Comb. Sci. Tech.* 78 (1991) 127-145.

[22] F.A. Vaz, A.L. deBortoli, *Mecánica Computacional Vol XXIX* (2010) 2655-2661.

[23] I. Glassman, *Combustion*, Academic Press, London, 2008, pp. 353,653.

[24] S.R. Turns, *An Introduction to Combustion,* McGraw Hill, New York (2000) 705.

[25] C.R. Shaddix, *Proceedings of the 33rd National Heat Transfer Conference* (1999) Aug 15-17 1-9

[26] D.C. Collis, M.J. Williams, *J. Fluid Mech.* 6 (1959) 357-384.

[27] M. Jakob, Heat Transfer, Vol. 1, Wiley, New York, 1949.

[28] G.G. Gubareff, J.E. Janssen, R.H. Torborg, *Thermal Radiation Properties Survey*, 2nd ed., Honeywell Research Center, Minneapolis-Honeywell Regulator Co., Minneapolis, 1960.

[29] A. S. Rangwala, S. G. Buckley and J. L. Torero, *Combust. Flame* 152 (2008) 401-414.

[30] Y. Pizzo, J.L. Consalvi, P. Querre, M. Coutin, L. Audouin, B. Porterie, J.L. Torero, *Combust. Flame* 152 (2008) 451-460.

[31] C.B. Jiang, J.S. T'ien, Y.H. Shih, *Proc. Combust. Inst.* 26 (1996) 1353-1360.

TABLES

Table 1. Verification of the correlation from Eq. 4 using average burning rates.

Fuel and Flow Conditions	Measured $\overline{\dot{m}}''_f$	Correlation $\overline{\dot{m}}''_f$	Error	B
Methanol Simulation (U = 0.5 m/s)	35.69 g/ m^{2}s	32.88 g/m^{2}s	7.87 %	2.7 [22]
Methanol Simulation (U = 1.0 m/s)	42.48 g/ m^{2}s	39.58 g/m^{2}s	6.83%	2.7 [22]
Methanol Simulation (U = 1.5 m/s)	48.89 g/ m^{2}s	45.64g/m^{2}s	6.65%	2.7 [22]
Methanol Simulation (U = 1.8 m/s)	53.22 g/ m^{2}s	51.42 g/m^{2}s	3.38%	2.7 [22]
Ethanol Simulation (U =0.5 m/s)	36.95 g/ m^{2}s	35.49 g/m^{2}s	3.95%	3.25 [22]
Methanol (Hirano, U= 0.5 m/s) [14]	34.56 g/ m^{2}s	36.76 g/m^{2}s	6.34%	2.7 [22]

Table 2. Physical properties

Properties	Methanol	Ethanol	PMMA
Mass transfer number, B	2.7 [22]	3.25 [22]	1.3 [2]
Thermal conductivity, k (W/m-K) evaluated at ambient temperature of 300 K	0.0263 [23]	0.0263 [23]	0.0263 [23]
Specific heat, c_p (J/kg-K) evaluated at the adiabatic flame temperature	1394.5 [23]	1417 [23]	1658.5 [23]
Length of the condensed fuel surface (m)	0.08	0.08	0.08

FIGURES

FIGURE 1

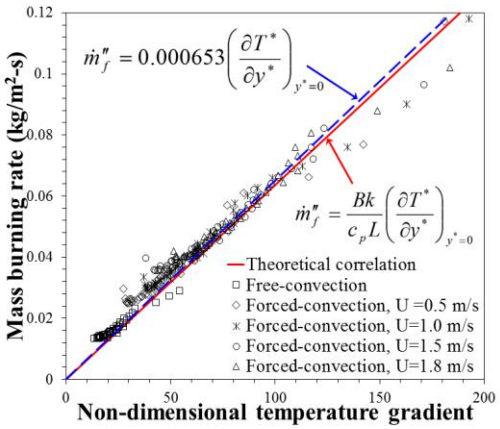

Figure 1: The local mass-burning rate per unit area vs. the non-dimensional temperature gradient at the fuel surface for numerical simulations of methanol flames under forced-convective and naturally-convective environments, with free-stream velocities *U* over a fuel surface of length 8 cm. The dashed straight line indicates the linear fit through numerical data points indicated by symbols whereas solid straight line indicates the theoretical fit.

FIGURE 2

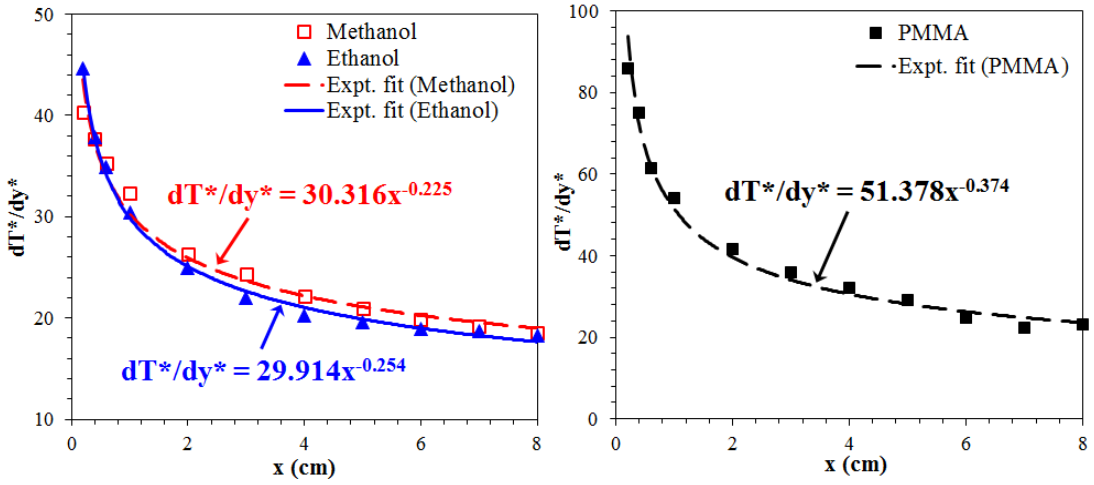

Figure 2: Variation of the non-dimensional temperature gradient at the methanol/ethanol condensed fuel surface (left) and PMMA surface (right) along its length.

FIGURE 3

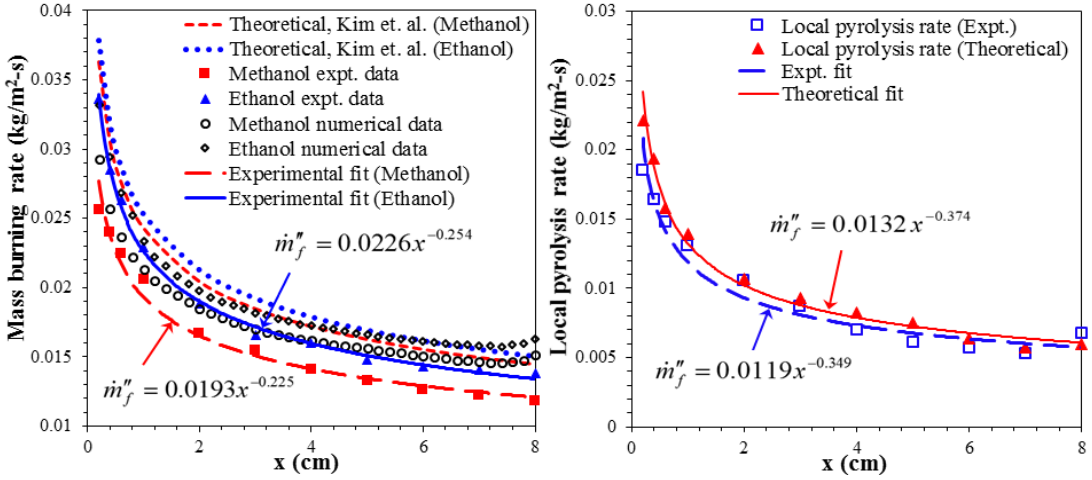

Figure 3: Variation of the local mass-burning rate over a methanol and ethanol (left) and PMMA (right) condensed fuel surface along its length.

FIGURE CAPTIONS

Figure 1: The local mass-burning rate per unit area vs. the non-dimensional temperature gradient at the fuel surface for numerical simulations of methanol flames under forced-convective and naturally-convective environments, with free-stream velocities *U* (m/s) over a fuel surface of length 8 cm. The dashed straight line indicates the linear fit through numerical data points indicated by symbols whereas solid straight line indicates the theoretical fit.

Figure 2: Variation of the non-dimensional temperature gradient at the methanol/ethanol condensed fuel surface (left) and PMMA surface (right) along its length.

Figure 3: Variation of the local mass-burning rate over a methanol and ethanol (left) and PMMA (right) condensed fuel surface along its length.

Supplemental material

1. Radiation correction

Flame temperature measurements across the width of the fuel sample showed no significant variation, except near the edges. Therefore, a single thermocouple at the center of the flame was used to produce a map of temperatures in the boundary layer by moving it across the flame (Y-direction) and along the length of the flame (X-direction). The temperature measurements reported in this study have been corrected for thermocouple radiation. In the most general case, an energy balance on the thermocouple junction takes the following form,

$$\dot{Q}_{cat} + \dot{Q}_{conv} + \dot{Q}_{rad} + \dot{Q}_{cond} = mc_p \frac{dT_{tc}}{dt} \tag{1}$$

with heat transfer associated with surface-induced catalytic reactions, convection between the gases and the thermocouple, radiant heat transfer between the thermocouple and its surroundings, conduction along the thermocouple wires, and transient heating or cooling of the thermocouple incorporated in Eq. (1). The thermocouple junction properties that characterize the transient term in the above expression include the mass m and the specific heat c_p. Both the conduction error and errors due to catalytic effects were estimated to be small in the given study, therefore they are neglected. For steady measurements, Eq. (1) reduces to a convective-radiative balance given by,

$$h(T_g - T_{tc}) = \varepsilon_{tc}\sigma(T_{tc}^4 - T_{surr}^4)$$

$$T_g - T_{tc} = \frac{\varepsilon_{tc} d\sigma}{kNu}(T_{tc}^4 - T_{surr}^4), \tag{2}$$

where T_g is the real gas temperature, T_{tc} is the thermocouple junction (or bead) temperature, T_{surr} is the temperature of the surroundings, ε_{tc} is the emissivity of the thermocouple junction, σ is the Stefan-

Boltzmann constant and h is the convective heat transfer coefficient of the flow over the thermocouple junction defined as $h = k\,\mathrm{Nu}/d$. k is the thermal conductivity of the gas, Nu is the Nusselt number, and d is the thermocouple wire diameter. The choice of the Nusselt number correlation is of paramount importance in calculating a radiation correction to the measured thermocouple temperature because, as shown in Eq. (2), the radiation correction is inversely proportional to the Nusselt number. This choice is complicated, however, due to the existence of multiple "appropriate" Nusselt number correlations and the difficulty in estimation of the properties of the gas mixture surrounding the thermocouple, particularly its thermal conductivity. The bulk of evidence in literature, however, clearly indicates that a cylindrical Nusselt number correlation is most appropriate for describing the convective heat transfer to nearly all practical thermocouples [1], preferably that of Collis and Williams [2]. A commonly-used expression from Collis and Williams can be written as [2],

$$Nu\left(\frac{T_m}{T_g}\right)^{-0.17} = 0.24 + 0.56\,\mathrm{Re}_d^{0.45} = 0.24 + 0.56\left(\frac{Ud}{\nu}\right)^{0.45} \tag{3}$$

which was obtained for 0.02 < Re < 44, with the Reynolds number evaluated at the so-called film temperature, T_m, the mean of the thermocouple and free-stream temperatures, i.e. $0.5\left(T_g + T_{tc}\right)$. Here, Re is the Reynolds number defined as indicated for the local gas flow velocity, U, and kinematic viscosity, ν. Substituting Eq. (3) into Eq. (2) and neglecting the small temperature dependence in Eq. (3), we have a system of two equations with two unknowns (namely T_g and U),

$$T_g - T_{tc_1} = \frac{\varepsilon_{tc_1} d_1 \sigma}{k[0.24 + 0.56(Ud_1/\nu)^{0.45}]}(T_{tc_1}^4 - T_{surr}^4) \tag{4}$$

$$T_g - T_{tc_2} = \frac{\varepsilon_{tc_2} d_2 \sigma}{k[0.24 + 0.56(Ud_2/\nu)^{0.45}]}(T_{tc_2}^4 - T_{surr}^4) \tag{5}$$

which demonstrates that the difference between a thermocouple reading and the actual gas temperature (i.e. the error in gas temperature measurement) increases for larger-diameter thermocouples, while it is reduced by increasing the gas flow velocity over the junction. In solving the above equations, iteration is required since the gas conductivity and kinematic viscosity is a function of the gas temperature. Initially the gas temperature is taken to be the bead temperature for the purpose of evaluating the thermal conductivity and kinematic viscosity; then, the approximate value of the gas temperature is used to re-evaluate the conductivity and viscosity.

The emissivity of the bead (ε_{tc}) can also be found as a function of its temperature. In an analysis outlined by Jakob [3], Maxwell's wave equations can be solved to yield the complex indices of refraction for a metal as a function of its electrical resistivity. In the limit of low resistivity and assuming a large index of refraction, which is true for metals, Jakob [3] gives the hemispherical total emissivity of platinum (Pt) as,

$$\varepsilon = 0.751(r_e T)^{1/2} - 0.396 r_e T, 0 < r_e T < 0.2 \tag{5}$$

where, for platinum, $r_e \approx r_{e,273} T / 273$, with T in K and $r_{e,273} = 11 \times 10^{-6}\,\Omega - cm$ [4]. Therefore, the platinum emissivity becomes

$$\varepsilon = 1.507 \times 10^{-4} T - 1.596 \times 10^{-8} T^2 \tag{6}$$

for $0 < T < 2230$ K. This equation is confirmed by comparison with experimental data shown in Fig. S1 [5]. For temperatures where radiation is important, predicted and observed emissivities agree to within 1%. The emissivity of the thermocouple bead or junction can therefore be evaluated by using the above expression. Note that iteration is not needed for the evaluation of the platinum emissivity, since this property is a function of the bead temperature, which is known.

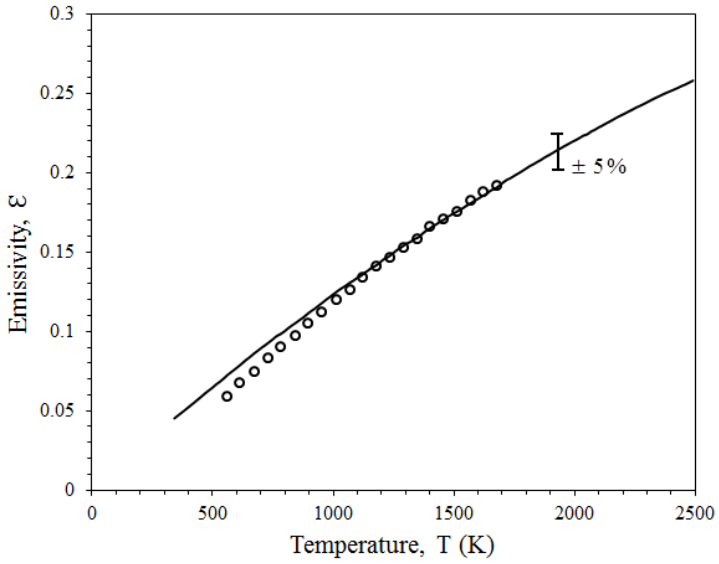

Figure S1. Total emissivity of platinum vs. temperature based on Jakob's theoretical calculation [3] (solid line) and experimental data from [2] (circular dots).

The actual gas temperature can then be evaluated by solving Eq. (4) and (5). During experiments, the two thermocouples were traversed exactly to the same measurement points and data was sampled to account for radiation correction in the temperature measurements. Compensated temperature profiles incorporating radiation corrections are shown in Fig. S2 for a methanol and an ethanol diffusion flame.

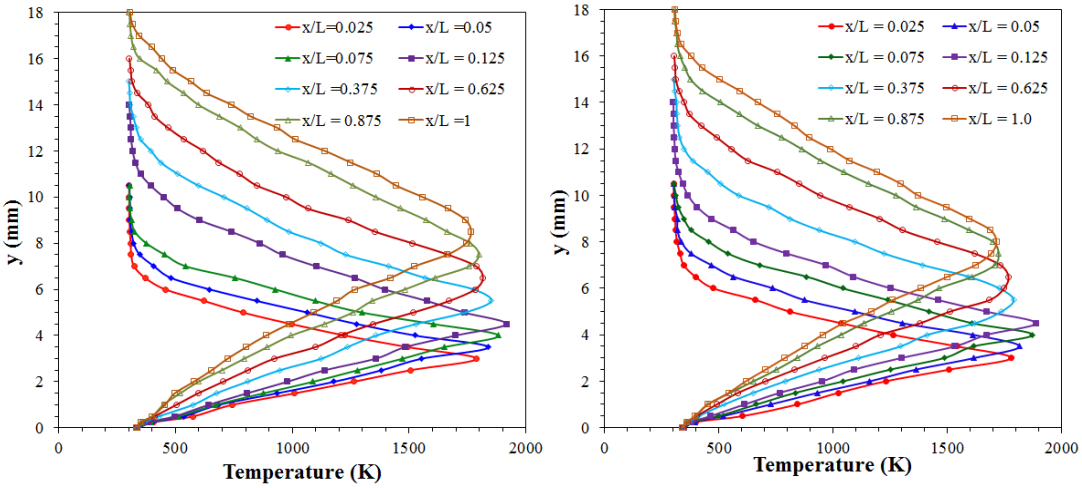

Figure S2: (left) Temperature profiles at several locations along the fuel surface of length 8 cm for a methanol diffusion flame. (right) Temperature profiles at several locations along the fuel surface of length 8 cm for an ethanol diffusion flame.

2. PMMA regression and local pyrolysis rate

Figure S3 (a) shows the regression profiles of the PMMA surface at different burn-out times. Significant regression was observed in the leading section when compared with regression at locations downstream. This was found to be consistent with the non-uniform rate of heat feedback from the boundary-layer flame to the PMMA surface. At higher burn-out times ($t > 250\,\text{s}$), the sample surface had receded significantly below the level of the original surface. This resulted in the formation of valley or a step in the leading section as shown in Fig. S3 (a). Fig. S3 (b) present the time-averaged regression rate at various stream-wise locations x.

Once steady burning was established the local pyrolysis mass-flow rate can be computed from the first-order approximation given by Pizzo et. al. [6], at each location x along the stream-wise direction,

$$\dot{m}''(x,t) = \rho_s \frac{d\delta}{dt} \approx \rho_s \frac{\delta(x,t+\Delta t) - \delta(x,t)}{\Delta t}, \tag{7}$$

where the PMMA density is taken to be 1190 kg/m^3 (from the manufacturer's mechanical property sheet). Derivatives in Eq. (7) should be computed with a smaller Δt in order to reduce approximation errors. However, at a smaller Δt, it becomes really difficult to measure the change in regression profiles accurately. This is primarily because the change in surface regression is small at lower Δt. Thus, the derivatives were computed using a time step of 50 s, long enough to detect a significant displacement of the regressing surface, but short enough to avoid surface swelling effects. The regression data for burn-out times of 100 and 150 s were used to evaluate the derivative in Eq. (7).

Ndubizu and co-authors [7] suggest that in the leading section of the solid, where the heat feedback is very high, steady state is attained soon after ignition (before a significant valley is formed). They noted that in that period, approximately all the heat feedback is used to gasify the solid. They found that at longer burn-out times, a valley is formed and the surface regression rate decreases with time. The same trend can be observed in Fig. S3 (b). This suggests that the heat reaching the surface in this section is no

longer steady at later times. Therefore, it becomes necessary to complete the temperature measurements during the initial stages of burning when the PMMA surface remains relatively flat. It was observed that the PMMA surface remains relatively flat up to a burn-out time of 150 s. We therefore chose the regression profiles at 100 and 150 s to compute the derivatives in Eq. (7) for the local pyrolysis rate.

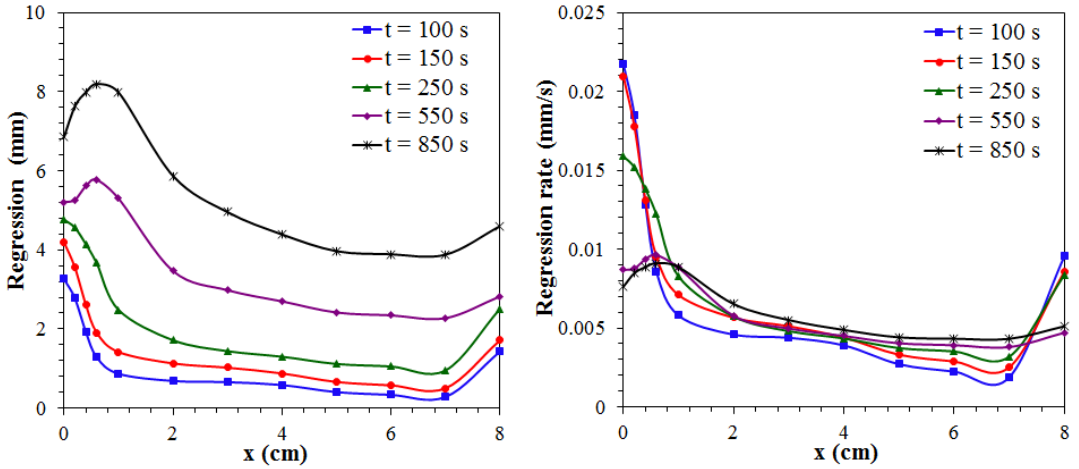

Fig. S3. (a) Regression profiles of the PMMA surface at different burn-out times (b) PMMA surface regresion rates at various stream-wise locations in tests lasting 100, 150, 250, 550 and 850 seconds.

[1] C.R. Shaddix, Proceedings of the 33rd National Heat Transfer Conference (1999) Aug 15-17 1-9

[2] D.C. Collis, M.J. Williams, *J. Fluid Mech.* 6 (1959) 357-384.

[3] M. Jakob, Heat Transfer, Vol. 1, Wiley, New York, 1949.

[4] C. D. Hodgeman (ed.), handbook of Chemistry and Physics, 42nd ed., CRC Pess, Cleveland, 1960

[5] G.G. Gubareff, J.E. Janssen, R.H. Torborg, Thermal Radiation Properties Survey, 2nd ed., Honeywell Research Center, Minneapolis-Honeywell Regulator Co., Minneapolis, 1960.

[6] Y. Pizzo, J.L. Consalvi, P. Querre, M. Coutin, L. Audouin, B. Porterie, J.L. Torero, *Combust. Flame* 152 (2008) 451-460.

[7] C.C. Ndubizu, R. Ananth, P. A. Tatem, *Combust. and Flame* 141 (2005) 131-148.